Designing concentric nanoparticles for surface-enhanced light-matter interaction in the mid-infrared

IRYNA KHODASEVYCH,[1,2] PATRICK RUFANGURA,[1,2] AND FRANCESCA IACOPI[1,2*]

[1]*School of Electrical and Data Engineering, Faculty of Engineering and IT, University of Technology Sydney, Broadway, 2007 NSW, Australia*
[2]*Australian Research Council Centre of Excellence on Transformative Meta-Optical Systems, University of Technology Sydney, Broadway, 2007 NSW, Australia*
** francesca.iacopi@uts.edu.au*

Abstract: Nanosized particles with high responsivity in the infrared spectrum are of great interest for biomedical applications. We derive a closed-form expression for the polarizability of nanoparticles made of up to three concentric nanolayers consisting of a frequency dependent polar dielectric core, low permittivity dielectric spacer shell and conductive graphene outer shell, using the electrostatic Mie theory in combination with conductive layer in a dipole approximation. We use the obtained formula to investigate SiC, GaN and hBN as core materials, and graphene as conductive shell, separated by a low-permittivity dielectric spacer. Three-layer nanoparticles demonstrate up to a 12-fold increased mid-infrared (MIR) absorption as compared to their monolithic polar dielectrics, and up to 1.7 as compared to two-layer (no spacer) counterparts. They also show orders of magnitude enhancement of the nanoparticle scattering efficiency. The enhancement originates from the phonon-plasmon hybridization thanks to the graphene and polar dielectric combination, assisted by coupling via the low permittivity spacer, resulting in the splitting of the dielectric resonance into two modes. Those modes extend beyond the dielectric's Reststrahlen band and can be tuned by tailoring the nanoparticles characteristics as they can be easily calculated through the closed-form expression. Nanoparticles with dual band resonances and enhanced absorption and scattering efficiencies in the MIR are of high technological interest for biomedical applications, such as surface -enhanced vibrational spectroscopies allowing simultaneous imaging and spectroscopy of samples, as well as assisting guided drug delivery.

OCIS codes: (290.4020) Mie theory; (300.6340) Spectroscopy, infrared; (160.4236) Nanomaterials; (250.5403) Plasmonics; (290.5850) Scattering, particles; (300.1030) Absorption; (170.4580) Optical diagnostics for medicine;

1. Introduction

Nanoparticles are particularly attractive for applications in surface-enhanced Raman spectroscopy (SERS) [1], surface-enhanced IR absorption (SEIRA) [2] and functionalization for tailored drug delivery [1]. Recently nanoparticles were proposed as injectable wireless neural activity nanosensors [3, 4]. Localized plasmon resonance, induced after irradiation of nanoparticle with light, provides near field enhancement that amplifies light-matter interaction and enables efficient functionalities using small quantities of nanoparticle material.

An efficient absorption is required for photothermal drug delivery [5], nanoparticle heat based and antibiotic free sterilisation [6], and nanoparticle hypothermia treatment. A high nanoparticle scattering cross-section is favourable for imaging-based nanoparticles as biomedical contrast agents [7-10], as it may help circumvent the need for fluorescent tagging. Other optical applications of core-shell nanoparticles involve radiative heat flux control [11, 12], photovoltaics for light trapping and increasing the efficiency of solar cells [13], and solar

thermal energy harvesting [14]. Coupling between molecular excitons and nanoparticles facilitates strong light-matter interactions for lasers and quantum networks [15]. In this work, we will emphasize the relevance for biomedical applications in the MIR.

There are three identified near-infrared (NIR) biological transparency windows that can be used for medicine: NIR-I (650–950 nm), NIR-II (1000–1350 nm), and NIR-III (1500–1800 nm).

The overwhelming majority of research and treatments so far has focused on metal plasmonic nanoparticles intended for operation in NIR-I range, where metal plasmonic nanoparticles like gold, silver, etc show exceptional response [16]. In-vitro techniques, such as surface-enhanced Raman spectroscopy, have reached unprecedented sensitivity where detection of one molecule is possible. Various coatings have been applied to metal nanoparticles for functionalization, stabilization, and improvement of biocompatibility. Benefits of two- and three-layer metal core-shell nanoparticles in the NIR-I have been investigated. Three-layer core-shell nanoparticles have distinctly different field distribution with the field tightly confined in thin middle shell or spacer layer, providing superior enhancement compared to two-layer particles [16]. Three-layer plasmonic metal nanoparticles have been proposed for gap-enhanced Raman tags (GERTs) demonstrating orders of magnitude higher SERS responses due to enhanced electromagnetic fields in the spacer gap [1].

In addition, when tags are placed within the spacer layer, they are protected from unwanted environmental effects and chemical or photo-chemical reactions. Also, tags located in the gap or spacer are protected from effects of nanoparticle aggregation and produce desired linear dependence of the signal on tag concentration. Multiplexing via loading the gap with a number of different tags is also possible. Nanoparticles can be further functionalised with targeting biochemicals for selective binding with biomolecules, such as tumours. For example, GERTs were used for intraoperative tumour imaging, when injected nanoparticles travel to and attach to tumour tissue and can be later seen during operation to identify tumour margins and ensure that all unhealthy tissue is removed.

Amongst in-vivo applications, theranostics is combined diagnostics and treatment and is very promising for cancer treatments. It uses nanoparticles functionalised with chemicals that target cancer cells and attach to them [7-9]. Plasmonic photothermal therapy uses irradiation and heating that occurs due to absorption of radiation by nanoparticles. Cancer cells are very sensitive to elevated temperatures, a moderate rise in temperature to only 40-44 °C is effective against tumours, while healthy tissue is unaffected [5]. Of particular interest are multipurpose nanoparticles when one regime can be used for imaging and drug release monitoring (off-resonance) and another regime for heating treatment or drug release via external shell photothermal rupture (on-resonance) [1]. However, penetration depth of NIR-I radiation through the human body is about 2 mm [17], thus limiting applications to shallow treatments, such as skin, ovarian and breast cancer.

New research focus is on NIR-II band, promising up to 2 cm penetration depth in biological tissues [18]. However, larger metal nanoparticles are needed for resonance in this band. One study indicates that gold nanorods up to 900 nm in length resonate in this band, but large nanoparticles tend to accumulate in the body [1, 19, 20]. Developing plasmonic nanoparticles and biotags for longer wavelengths of operation while keeping them small is challenging and emerging field of research.

Although penetration depth of external mid- and far-infrared radiation through the skin is limited to a superficial skin layer of 500 μm [10, 17], the body itself is a good emitter and absorber of infrared radiation around 10 μm, corresponding to its black body temperature. So, new heat-based treatments, triggered by the body's own radiation after injection can be devised. Reduced scattering from biological tissues at mid-infrared (MIR) makes it also better suited for coherent imaging and 3D holography of molecules with high spatial resolution.

The MIR spectrum is rich with chemical and biological absorption resonances [21-23], for example O-H, N-H, C=O, C-C, CH_2, CH_3 bonds, water, proteins, lipids, as well as gasses like

CO_2, CH_4. In contrast to indirect detection, where SERS tags serve as labels, a direct identification of the vibration information of molecules is used in surface-enhanced IR absorption SEIRA. Combining SERS and SEIRA approaches is also of interest, as it allows simultaneous imaging and spectroscopy of samples. Metallic nano/microstructures are traditionally used for concentrating the incident radiation and improving the overlap of the field with molecules, thus enhancing the interaction. As with SERS, micrometre sized metal structures are required for resonances in MIR. Field confinement to nanosized hotspot is required for detection of small amounts of substances with sufficient spatial resolution. Bowtie gold structures with 3 nm gap achieved minimum 500 molecules detection [2]. However, single molecule detection is still beyond reach for SEIRA. Translating the knowledge on nanostructure design from the optical domain to MIR is important, however very few publications exist on nanoparticles for MIR.

MIR plasmonic and polaritonic materials, such as III–V semiconductors and 2D materials, such as MoS_2, WSe2, WS2, layered transition metal dichalcogenides (LTMDCs) and 2D hBN are a natural choice. Polar dielectrics, such as SiC, GaN, hBN, exhibit metallic type behaviour within their corresponding Reststrahlen bands in MIR due to excitation of localized surface phonon polaritons and are low-loss materials [24]. Thus, polar dielectrics at MIR can behave in an analogous to metals in the optical regime, they indicate lower losses as compared to metal plasmonics, however their responsivities are confined to a specific restricted band (Reststrahlen). SiC, GaN, hBN are all biocompatible and can be a suitable alternative to metal nanoparticles for biomedical applications. Also, importantly for in-vivo applications, nanoresonators made out of these materials are nanometer sized for the MIR operation (unattainable with metal particles). Some work was done to investigate application of polar dielectrics in the biomedical field, for example, SiC nanoparticles have been chemically modified to enable cancer-cell-specific labelling [7] and used as fluorescent biomarkers for cell monitoring or drug delivery [25].

Graphene is a preferred shell material, it is biocompatible and supports strongly confined localized plasmon modes in MIR that couple to phonons in polar dielectrics [26], extending resonant response beyond the Reststrahlen band. Fabrication methods exist for SiC/graphene nanostructures [26-28], where ultrathin silicon oxycarbide (SiOC) layer [27, 29] forms between SiC and graphene naturally and serves as a coupling low dielectric spacer layer. Graphene can be electrostatically tuned to sweep continuously over various vibrational bands [30-32]. It has been investigated for enhancing or tuning metal nanoparticles [33, 34], however lately it is gaining popularity on its own, as was demonstrated in a number of biosensors [35, 36].

There is therefore interest in designing complex graphene-coated nanoparticles in the MIR range. However, the majority of formulae for calculations of polarizability is usually limited to one or two layers, such as nanoparticle on its own or with one nanoshell. Two-layer graphene coated nanoparticles were theoretically analysed in [11, 37]. Recent works on multilayered graphene nanoshells based on Mie theory are fairly complex [38, 39], include higher order modes not usually required in biomedical applications and complex mathematical functions. There is a need for a simplified three-layer model that is easy to use.

In this paper, we first derive general easy to use analytical formula for the polarizability of a three-layer nanoparticle, using the dipole approximation of Mie theory with a conductive boundary. Then we use the expression to compare the polarizability, absorption and scattering efficiencies of three-layer graphene coated nanoparticles with SiC, GaN and hBN, cores and graphene shell. We show the benefits of using a sandwiched layer between the core and the graphene shell of low permittivity oxide, which acts as coupling medium. We provide guidelines for the nanoparticle design and demonstrate enhanced capabilities for absorption and scattering. Lastly, we confirm the validity of the derived analytical expression by modelling the nanoparticles with 3D Comsol Multiphysics simulations [40].

2. Theoretical background

Figure 1(a) shows the proposed three-layer polar dielectric (core)/dielectric (spacer) /2D plasmonic material (shell) nanoparticle immersed in a generic host medium, excited with a plane wave mid-infrared electromagnetic field. The host medium with permittivity ε_h could be air or other dielectric, representing immersion in a chemical solution that needs testing. The nanostructure consists of a polar dielectric core nanosphere of radius r_1 and permittivity $\varepsilon_1(\omega)$, a dielectric low permittivity spacer layer with thickness $d=r_2-r_1$ and permittivity ε_2, and 2D monolayer conductive nanoshell of infinitesimal thickness and conductivity $\sigma(\omega)$.

For a better understanding of the origin of resonances and behaviour of the multilayered nanoparticle, its response is compared to the responses of the core nanosphere and two-layer polar dielectric (core) /2D monolayer conductor (shell) nanoparticle that contribute to its response. SiC, GaN and hBN polar dielectrics were investigated with graphene shell as 2D plasmonic conductor. The investigations were conducted in the wavelength range between 5-20 μm, where the Reststrahlen bands between transverse (TO) and longitudinal (LO) optical phonon frequencies of the polar dielectrics are located.

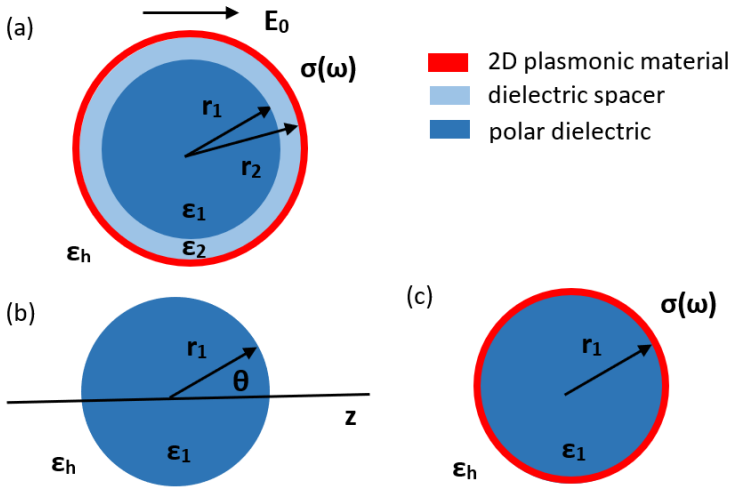

Fig. 1. Schematic of spherical nanoparticles immersed in a host dielectric medium (ε_h) and subject to an external electric field E_0: (a) a three-layer polar dielectric (core)/dielectric (spacer) /2D plasmonic material (shell), (b) polar dielectric sphere, (c) a two-layer polar dielectric (core)/2D plasmonic material (shell).

First, we derived a closed-form simplified analytical formula expressing the electric polarizability for three-layers polar dielectric (core)/dielectric (spacer)/2D monolayer conductor (shell) nanosphere shown in Fig.1(a) for dipole mode. The full derivation details and Matlab Symbolic Math Toolbox code used for working with expressions in analytical form are provided as supplementary material. The resonant frequencies of the nanostructure then can be calculated as poles of polarizability.

The derived formula is very general and allows for ideal dielectrics, lossy dielectrics and metal type materials to be used for permittivities ε_1 and ε_2. However, the assumption is a spatially isotropic material. The 2D material is treated as an infinitesimally thin conductive boundary, requiring consideration of charges or current on the boundary. Note that a conventional metal of a few nm thickness, which is less than skin depth or plasmon depth at MIR wavelength, can also be treated as an infinitesimally thin conductive boundary.

In order to investigate the response of the multilayered nanoparticles to the incident radiation, the scattering problem was solved. Due to the curved nature of nanoparticles,

localized plasmon and phonon resonances can be excited by plane wave illumination. The nanoparticles considered in this paper are deeply subwavelength at the infrared frequency range, so the electrostatic approximation can be used (also known as Lorenz-Mie theory). This means that spatial retardation effects were not considered, as the incident field does not change significantly across the diameter of the particle and both field amplitude and phase can be assumed constant across the particle. The frequency dependence of the field can be added later once the solution is obtained. The frequency dependence of polarizability manifests itself via the material parameters of the polar dielectrics and the 2D material. For this calculation, the 2D material was chosen to be graphene. All materials are considered to be nonmagnetic materials. The SI system of units and exp(-iωt) time-dependence are used in the paper.

Polarizability formulae for a single sphere and a two-layer core/shell sphere are reported in electromagnetics text books and previous publications [41-43]. The following formulae were used in calculations for polar dielectric core nanosphere in a dielectric host medium as shown in Fig.1(b):

$$\alpha(\omega) = 4\pi r_1^3 \frac{\varepsilon_1 - \varepsilon_h}{\varepsilon_1 + 2\varepsilon_h}, \tag{1}$$

For two-layer polar dielectric (core) /2D monolayer conductor (shell) nanoparticle as in Fig.1(c) the following formula was used [37]:

$$\alpha(\omega) = 4\pi r_2^3 \frac{\varepsilon_1 - \varepsilon_h + 2g}{\varepsilon_1 + 2\varepsilon_h + 2g}, \tag{2}$$

$$g(\omega) = \frac{i\sigma(\omega)}{\varepsilon_0 \omega r_2}, \tag{3}$$

where ε_0 is permittivity of free space, ω is the angular frequency of the incident wave.

In order to extend the approach to three-layer nanosphere as in Fig.1(a) we combined the electrostatic approach used to derive (1) with conductive boundary treatment of the 2D conductor shell (graphene, in this case) in (2). The electrostatic solution to Laplace equation for electric potential $\nabla^2 \Phi = 0$ is in the form of

$$\Phi(r,\theta) = \sum_{l=0}^{\infty} \left[A_l r^l + B_l r^{-(l+1)}\right] P_l(cos\theta), \tag{4}$$

where $P_l(cos\theta)$ are the Legendre polynomials of the order l and θ is the angle between the direction of the incident field $\boldsymbol{E_{inc}} = E_0 e^{-i\omega t}\hat{\boldsymbol{z}}$ and the observation point, where $\boldsymbol{E} = -\nabla\Phi$. Dipole mode corresponds to l=1, where $P_1(cos\theta) = cos\theta$. A and B are coefficients corresponding to electric potentials of the fields in each layer that are found by applying boundary conditions:

$$\boldsymbol{n} \times (\boldsymbol{E_n} - \boldsymbol{E_{n+1}}) = 0, \qquad \boldsymbol{n} \times (\boldsymbol{H_n} - \boldsymbol{H_{n+1}}) = \boldsymbol{J_n}, \tag{5}$$

where $\boldsymbol{J} = \sigma \boldsymbol{E}$ is surface current, $\boldsymbol{n}$ is the normal to the surface of the sphere and n, n+1 are the indexes of the layers. The derived expression for a three-layer nanoparticle with a conductive boundary is:

$$\alpha(\omega) = 4\pi r_2^3 \frac{(\varepsilon_2 - \varepsilon_h + 2g)(\varepsilon_1 + 2\varepsilon_2) + f(\varepsilon_1 - \varepsilon_2)(\varepsilon_h + 2\varepsilon_2 - 2g)}{(\varepsilon_2 + 2\varepsilon_h + 2g)(\varepsilon_1 + 2\varepsilon_2) + 2f(\varepsilon_1 - \varepsilon_2)(\varepsilon_2 - \varepsilon_h - g)}. \tag{6}$$

Scattering, absorption and extinction cross sections and efficiencies are the primary parameters of interest for nanoparticle applications. We calculate and compare these parameters for all the types of nanoparticles shown in Fig.1 using the following formulae:

$$C_{abs} = kIm(\alpha), \qquad C_{scat} = k^4 |\alpha|^2 / 6\pi,$$

$$Q_{abs} = C_{abs}/\pi r_2^2\,, \qquad Q_{scat} = C_{scat}/\pi r_2^2, \tag{7}$$
$$C_{ext} = C_{abs} + C_{scat}, \qquad Q_{ext} = C_{ext}/\pi r_2^2,$$

where C_{abs}, C_{scat} and C_{ext} are absorption, scattering and extinction cross sections, $k = \omega n/c$ is wavenumber of the incident wave in the host medium, ω is angular frequency, n is refractive index of the host medium, $Im(\alpha)$ is imaginary part of polarizability, Q_{abs}, Q_{scat} and Q_{ext} are absorption, scattering and extinction efficiencies.

Both polar dielectric permittivity and 2D plasmonic material conductivity are frequency dependent parameters. The permittivity of polar dielectrics can be described by the formula:

$$\varepsilon(\omega) = \varepsilon_\infty \left(1 + \frac{\omega_{Lo}^2 - \omega_{To}^2}{\omega_{To}^2 - \omega^2 - i\gamma\omega}\right), \tag{8}$$

where ε_∞ represents the high-frequency permittivity, ω_{TO} and ω_{LO} are the TO and LO phonon frequencies, and γ is the damping constant associated with optical phonon. Three polar materials, cubic SiC (3C-SiC), GaN and hBN, were investigated.

For 3C-SiC the values $\omega_{TO} = 797\ \text{cm}^{-1}$ and $\omega_{LO} = 973\ \text{cm}^{-1}$, $\varepsilon_\infty = 6.52$, and $\gamma = 12\ \text{cm}^{-1}$ were used from the measured data in [26]. For GaN $\omega_{TO} = 533\ \text{cm}^{-1}$ and $\omega_{LO} = 744\ \text{cm}^{-1}$, $\varepsilon_\infty = 5.35$, and $\gamma = 17\ \text{cm}^{-1}$ were used as representing the properties along the normal direction of the GaN crystal. In tangential direction the values are $\omega_{TO} = 560\ \text{cm}^{-1}$ and $\omega_{LO} = 746\ \text{cm}^{-1}$, $\varepsilon_\infty = 5.35$, and $\gamma = 17\ \text{cm}^{-1}$, e.g. differ substantially only in location of TO [44], hence only normal direction properties were used for further calculations. There are two Reststrahlen bands for hBN, which are significantly away from each other. For normal direction (excitation by incident field parallel to anisotropy axis) the values are $\omega_{TO} = 1360\ \text{cm}^{-1}$ and $\omega_{LO} = 1614\ \text{cm}^{-1}$, $\varepsilon_\infty = 4.9$, and $\gamma = 7\ \text{cm}^{-1}$, and for tangential direction (excitation by incident field perpendicular to anisotropy axis) $\omega_{TO} = 760\ \text{cm}^{-1}$ and $\omega_{LO} = 825\ \text{cm}^{-1}$, $\varepsilon_\infty = 2.95$, and $\gamma = 2\ \text{cm}^{-1}$ [45]. Separate calculations were conducted for the normal and the tangential cases of hBN.

As we chose monolayer graphene as the 2D conductor shell, its conductivity σ(ω) was calculated using the Kubo formula, expressed by the sum of interband (σ_{intra}) and intraband (σ_{inter}) transitions [12]

$$\sigma_{intra} = \frac{2ie^2 k_B T}{\pi\hbar^2\,(\omega + i\tau^{-1})}\, ln\left[2cosh\left(\frac{E_F}{2k_B T}\right)\right], \tag{9}$$

$$\sigma_{inter} = \frac{e^2}{4\hbar}\left[\frac{1}{2} + \frac{1}{\pi}arctan\left(\frac{\hbar\omega - 2E_F}{2k_B T}\right) - \frac{i}{2\pi}\, ln\frac{(\hbar\omega + 2E_F)^2}{(\hbar\omega - 2E_F)^2 + (2k_B T)^2}\right], \tag{10}$$

$$\sigma(\omega) = \sigma_{intra} + \sigma_{inter}, \tag{11}$$

where k_B and $\hbar$ are the Boltzmann and reduced Planck constant, respectively, e is the electron charge. For the sake of the analytical and numerical calculations in this work, we selected a Fermi level of $E_F = 0.37$ eV as representative of a graphene on silicon carbide with a thin oxide spacer [46] and $\tau = 370\ fs$ as relaxation time estimate for graphene at room temperature [30, 46-48]. The conductivity of graphene can be tuned via altering its Fermi level, which can for example be controlled by electrostatic gating. Other 2D plasmonic materials can be described by a similar approach.

3. Nanoparticle analysis

Three-layer nanoparticles with SiC, GaN and two variations of hBN cores were investigated and compared. For all nanoparticles total radius of all the layers r_2 =25 nm, polar dielectric core radius r_1 = 17.5 nm and low permittivity dielectric spacer has thickness d=7.5 nm and permittivity ε_2 =2.25. Nanoparticles have outer graphene shell and are located in air with permittivity ε_h=1. Table I summarises the results.

Figures 2(a)-(d) compare polarizabilities for nanoparticles from Fig.1 with various polar dielectric cores. The green curves represent polarizability of a monolithic sphere in air (as in Fig.1(b)). The localized phonon resonance occurs within the Reststrahlen band when $\varepsilon_1 = -2\varepsilon_h$. The polar dielectric's permittivity is frequency dependent and coating such dielectric sphere with a graphene shell (two-layer particle in Fig.1(c)) results in the splitting of the resonance into two modes. The splitting is due to the hybridization of the localized surface plasmon of the graphene shell and the surface phonon resonance of the polar dielectric core (black curve). This type of hybridization has been studied extensively for metallic core-shell nanoparticles [16, 49]. It was shown that the interaction between the core material plasmon and the shell cavity plasmon generates one bonding and one antibonding mode, where electric fields in the core and the shell orient themselves symmetrically or anti-symmetrically, respectively. This concept was recently extended to the interaction of plasmon and surface phonon in SiC-graphene core-shell nanowires [26]. The mode splitting phenomenon can be beneficial for dual -band or dual -function operation. The shorter wavelength mode 2 (M2), exhibits an order of magnitude stronger polarizability than the mode 1 (M1) for SiC, GaN and hBN⊥ cores, and is 2 times stronger for hBN∥.

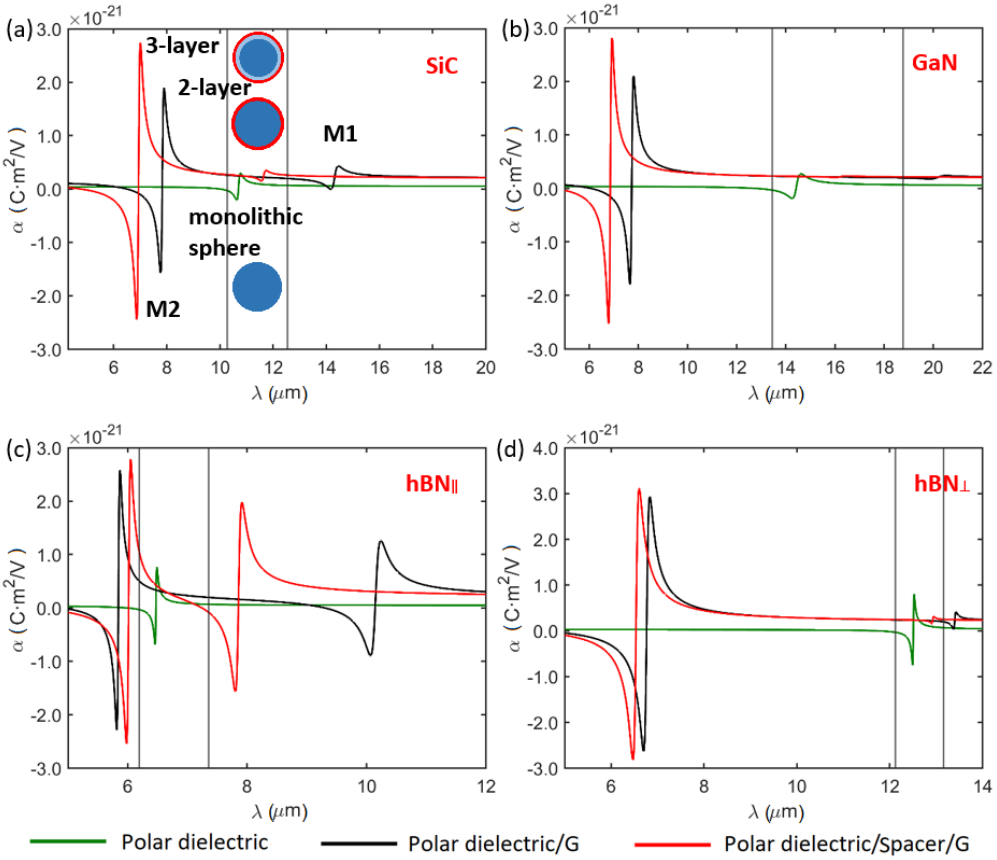

Fig. 2. Calculated polarizabilities for nanoparticles with polar dielectric cores as shown on labels, $r_1 = 17.5$ nm, $d = 7.5$ nm, $\varepsilon_2 = 2.25$, all particles are in air. The green spectra correspond to the monolithic polar dielectric sphere, the black spectra are for two-layer polar dielectric sphere/graphene shell, the red ones are for three-layer polar dielectric sphere/spacer/graphene shell. The black vertical lines show the location of Reststrahlen bands. Three-layer nanoparticles consistently show the highest polarizability in all cases.

Also, all three-layer nanoparticles (red curves) show mode splitting and demonstrate higher polarizability for M2 as compared to two-layer particles - about 1.3-1.4 times for SiC, GaN and hBN ∥ (hBN ⊥ remains roughly constant), and nearly an order of magnitude higher polarizability compared to monolithic nanoparticles.

It should be noted that although all monolithic nanospheres resonate at different wavelengths and polar dielectrics have Reststrahlen bands of different widths and in different spectral locations, the modes of three- and two-layer nanoparticles appear all within the same narrow ~6-8 μm window. This seems to indicate a predominance of the graphene response for the concentric nanoparticles.

Figures 3(a)-(d) compare absorption efficiencies for nanoparticles with various polar dielectric cores. Three-layer nanoparticles demonstrate absorption efficiency enhancements of up to 1.7 times over two-layer structures, and up to 12 times over monolithic spheres (mode M2). Interestingly, SiC and GaN cores lead to substantially stronger enhancements than hBN. Graphs of the calculated scattering efficiencies are shown in Fig. S3 (supplemental document), and corresponding details are also summarized in Table I.

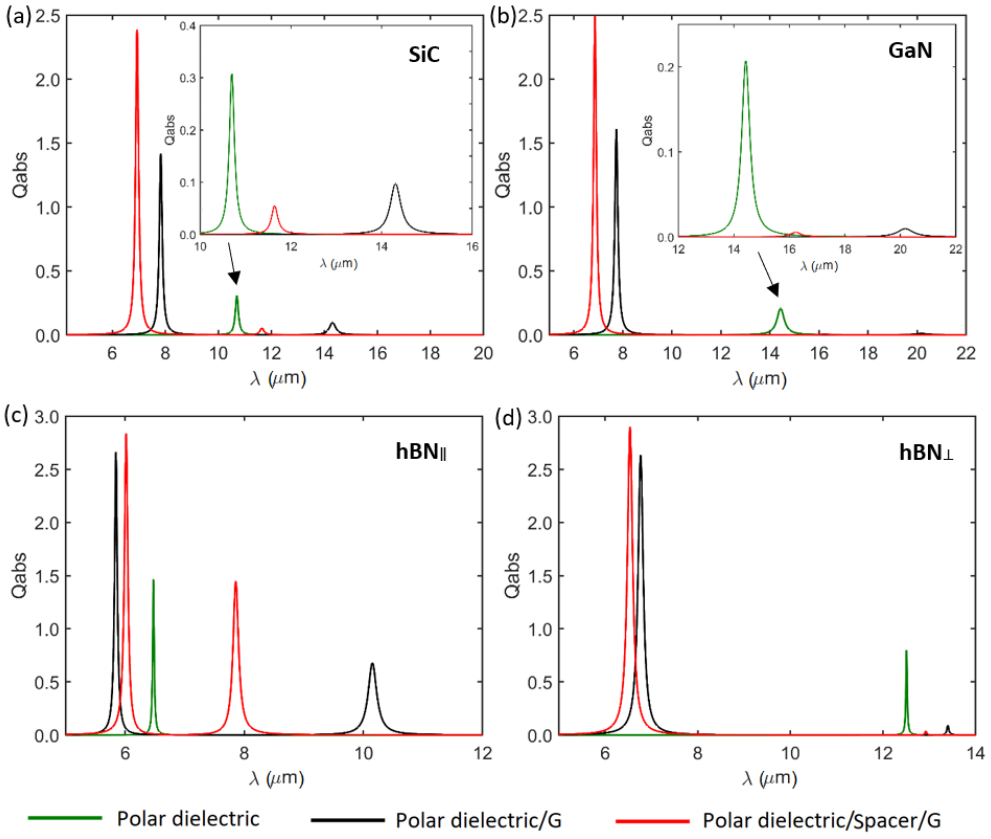

Fig. 3. Calculated absorption efficiencies for nanoparticles with polar dielectric cores as shown on labels, $r_1 = 17.5$ nm, $d = 7.5$ nm, $\varepsilon_2 = 2.25$, all particles are in air. The green spectra correspond to the monolithic polar dielectric sphere, the black spectra are for two-layer polar dielectric sphere/graphene shell, the red ones are for three-layer polar dielectric sphere/spacer/graphene shell. Three-layer nanoparticles consistently show the highest absorption efficiencies for all cases.

Table 1. Summary of analytically calculated resonant wavelengths (λ), polarisabilities (Re(α), absorption (Q_{abs}) and scattering (Q_{scat}) efficiencies maxima, numerically modelled resonant wavelengths (λ) and absorption A. The estimated enhancement ratios for three-layer versus two-layer and monolithic nanoparticles are also reported. G stands for graphene (shell) and Sp indicates the low-permittivity spacer with a chosen dielectric constant of 2.25.

	Analytical					Modelled (Comsol)	
Nanoparticles and modes	λ (μm)	Re(α)	λ (μm)	Q_{abs}	Q_{scat}	λ (μm)	A
SiC sphere	10.8	$3.0x10^{-22}$	10.7	0.3	$1.7x10^{-6}$	10.7	$2.2x10^{-3}$
SiC/G M1	14.5	$4.3x10^{-22}$	14.3	0.1	$2.7x10^{-7}$	14.6	$1.7x10^{-2}$
SiC/G M2	7.9	$1.9x10^{-21}$	7.8	1.4	$1.4x10^{-4}$	8.0	$2.2x10^{-2}$
SiC/Sp/G M1	11.7	$3.5x10^{-22}$	11.6	0.1	$3.0x10^{-7}$	11.6	$1.6x10^{-3}$
SiC/Sp/G M2	7.0	$2.7x10^{-21}$	6.9	2.4	$4.9x10^{-4}$	7.0	$6.5x10^{-2}$
Enhancement 3vs2/ 3vs1 layers				1.7 / **7.8**	3.6 / **290**		2.9 / **30.3**
GaN sphere	14.6	$2.7x10^{-22}$	14.4	0.2	$4.2x10^{-7}$		
GaN/G M1	20.5	$2.4x10^{-22}$	20.2	0.01	$1.4x10^{-8}$		
GaN/G M2	7.8	$2.1x10^{-21}$	7.7	1.6	$1.8x10^{-4}$		
GaN/Sp/G M1	16.5	$2.3x10^{-22}$	16.2	$0.6\ x10^{-2}$	$3.2x10^{-8}$		
GaN/Sp/G M2	6.9	$2.8x10^{-21}$	6.9	2.5	$5.4x10^{-4}$		
Enhancement 3vs2/ 3vs1 layers				1.6 / **12**	3.0 / **1290**		
$hBN_{\parallel}$ sphere	6.5	$7.7x10^{-22}$	6.5	1.5	$1.0x10^{-4}$		
$hBN_{\parallel}$/G M1	10.2	$1.3x10^{-21}$	10.2	0.7	$1.9x10^{-5}$		
$hBN_{\parallel}$/G M2	5.9	$2.6x10^{-21}$	5.8	2.7	$8.5x10^{-4}$		
$hBN_{\parallel}$/Sp/G M1	7.9	$2.0x10^{-21}$	7.9	1.4	$1.4x10^{-4}$		
$hBN_{\parallel}$/Sp/G M2	6.1	$2.8x10^{-21}$	6.0	2.8	$9.1x10^{-4}$		
Enhancement 3vs2/ 3vs1 layers				1.1 / **1.9**	1.1 / **8.9**		
$hBN_{\perp}$ sphere	12.5	$8.0x10^{-22}$	12.5	0.8	$8.5x10^{-6}$		
$hBN_{\perp}$/G M1	13.4	$4.2x10^{-22}$	13.4	0.1	$3.1x10^{-7}$		
$hBN_{\perp}$/G M2	6.8	$2.9x10^{-21}$	6.8	2.6	$6.2x10^{-4}$		
$hBN_{\perp}$/Sp/G M1	12.9	$3.2x10^{-22}$	12.9	0.04	$1.6x10^{-7}$		
$hBN_{\perp}$/Sp/G M2	6.6	$3.1x10^{-21}$	6.5	2.9	$8.1x10^{-4}$		
Enhancement 3vs2/ 3vs1 layers				1.1 / **3.6**	1.3 / **95**		

Enhanced absorption would lead to more efficient heating thus reducing the requirement on the power of the radiation source for photothermal treatments. As the result of enhanced electromagnetic fields, it is also expected to lead to better field-matter interaction and improved sensitivity of tag-based and tagless spectroscopy, such as SERS and SEIRA. As expected, absorption efficiency Q_{abs} is orders of magnitude higher than scattering efficiency Q_{scat} in all nanoparticles and dominates in the total extinction efficiency of the nanoparticles. Scattering is required for imaging and tag-based spectroscopy relying on emissions. Combining spectroscopy and imaging capabilities in one nanoparticle is an emerging area of interest for

SERS and SEIRA. It would allow to detect chemicals of interest and simultaneously observe their movements and interactions with other present substances.

Finally, in order to guide the design of the concentric particles, we have also conducted a parametric analysis for three-layer nanoparticles with a SiC core to illustrate dependencies on the radius of the core sphere r_1 = 12.5-125 nm, thickness of the dielectric shell d = 5-25 nm, permittivity of the shell ε_2 = 2-4 and host media ε_h = 1-4. We studied the effect of each parameter on the magnitude and wavelength of the peak of absorption cross section of the strongest hybridized mode M2 (Fig. 4). The absorption cross section magnitude shows monotonic dependence versus r_1, d and ε_h, such as increasing any of these parameters enhances absorption. Dependence of resonance on ε_h informs sensing capabilities in different media and indicates that the discussed absorption enhancement is higher in other media than air. It is also inversely dependent on ε_2, hence a low permittivity spacer is key. Resonant wavelengths corresponding to the peak of absorption show monotonic proportional dependence on all parameters except the core radius, where a saturation is reached for larger cores. Absorption cross sections for polar dielectric -based nanoparticles at MIR are comparable with plasmonic metal nanoparticle in the corresponding optical and NIR operating range and thus are highly suitable for biomedical applications in the previously unattainable MIR range. More detailed parametric analysis of one-, two-and three- layer graphene and SiC core nanoparticles at M1 and M2 modes is available in supplemental document.

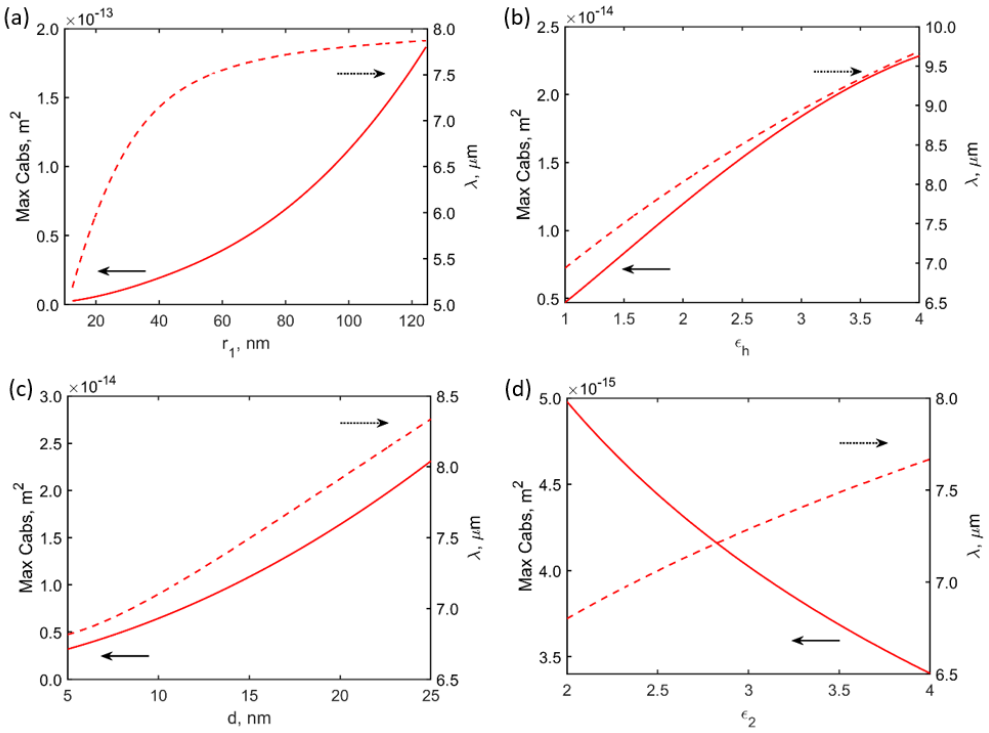

Fig. 4. Dependence of the absorption cross sections peak (solid line) and resonant wavelength (dotted line) of three-layer SiC nanoparticle mode M2 on (a) core radius r_1, (b) permittivity of the surrounding media ε_h, (c) dielectric shell thickness d, (d) permittivity of the spacer ε_2. Parameters that were kept constant during sweep had values r_1 = 17.5 nm, d = 7.5 nm, ε_2 = 2.25, ε_h = 1.

4. FEM Simulation

In order to validate the analytical expression, we have derived in this work, numerical simulations of concentric nanoparticles with a SiC core were performed using full-wave 3D simulations in COMSOL Multiphysics RF Module [40], which is based on finite element method. Graphene was simulated as a 2D conductive layer using a transition boundary condition and conductivity as per Eq. (9-11), which considers the thickness of the graphene layer and its dielectric properties. The model was excited with a plane electromagnetic wave. Nanoparticles were simulated as periodic lattice starting from a very low filling factor of 1% up to a densely packed particle array of about 90% filling factor. Note that negligible particle interaction is found below a 50% filling factor, where each particle behaves largely as a single distinct nanostructure, so the total array absorption is simply a summation of the single particles' absorptions. The absorption was calculated as A=1-R-T, where R and T are the reflectance and the transmittance intensities extracted from the simulations (Fig.5(a)). Excellent agreement between the analytical calculations (Q_{abs}) and 3D simulations (A) is observed both in terms of wavelengths at which resonances are found, and absorption trends, as summarised in Table I.

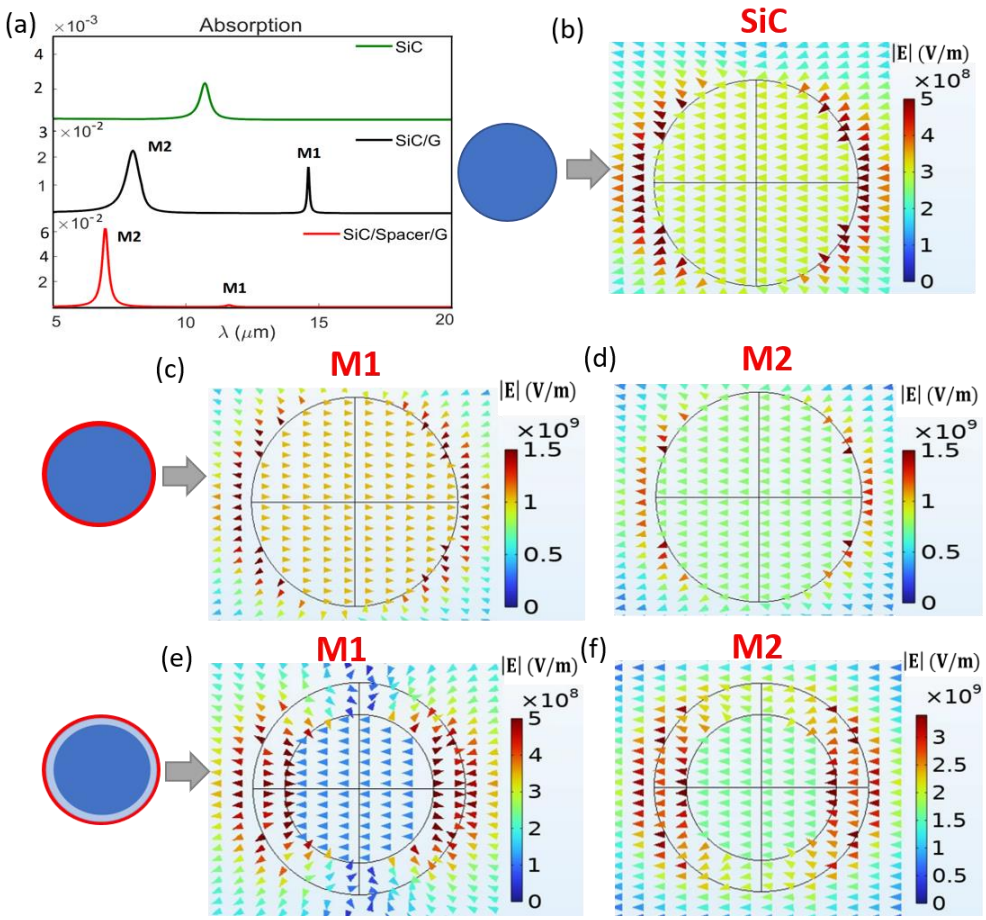

Fig. 5. (a) Simulations of absorption for one, two- and three-layer nanoparticle arrays in air with periodicity of 200 nm, ie 25% filling factor. (b) Simulated vector field distributions for the single mode of a SiC monolithic sphere, (c) mode M1 of SiC/G, (d) mode M2 of SiC/G, (e) mode M1 of SiC/Spacer/G, (f) mode M2 of SiC/Spacer/G.

We also investigated near-field responses, as shown in Fig.5. The monolithic SiC nanosphere exhibits dipole phonon resonance, as shown on the vector field plot. Coating the sphere by a plasmonic graphene shell in a 2- layer structure gives rise to two hybridized modes with symmetric and anti-symmetric field orientations. In both the cases the strongest field is outside the nanoparticle and non-negligible field is also present within the SiC core. When the third layer is added in the form of low dielectric coupling spacer, the field retains symmetric and anti-symmetric orientations for M2 and M1 correspondingly, but reaches its peak within the spacer layer, with M2 mode demonstrating the highest field magnitude.

5. Conclusion

In this work we have derived an easy-to-use analytical polarizability formula for up to three-layer polar dielectric (core) /dielectric (spacer) /2D monolayer conductor (shell) nanoparticles in dipole approximation. Calculations through this formula are in excellent agreement with calculation intensive 3D full-wave FEM modelling using Comsol Multiphysics.

Using this formula, we compare polarizabilities, absorption and scattering efficiencies of one, two- and three-layer nanoparticles with 3C-SiC, GaN and hBN cores and a graphene outer shell in the MIR spectral range, which includes the Reststrahlen bands of the corresponding polar dielectrics. Using a low-permittivity dielectric spacer, the MIR absorption and scattering efficiencies of three-layer nanoparticles are enhanced, as compared to both two-layer and monolithic nanoparticles. While the enhancement for two-layer nanoparticles is attributed to the hybridization of the surface plasmon and phonon polaritons of the graphene shell and polar dielectric cores, the further enhancement for the three-layer particles is attributed to the low permittivity spacer, acting as a coupling medium between the core and the shell of the nanoparticles.

The MIR spectrum is a promising area for nanoparticle -based biomedical applications, such as multipurpose functionalisation and photothermal drug delivery, antibiotic free sterilisation, hypothermia treatment, gap-enhanced tags and intraoperative tumour imaging with nanoparticles as biomedical contrast agents. Conventional metal particles are not suitable here, as they would need to be in the microns size range to be responsive in the MIR, hence they would tend to accumulate in the body in in-vivo studies. The discussed semiconductor and graphene concentric nanoparticles are a suitable alternative to micrometer- sized metal particles, offering enhanced absorption and increased sensitivity.

The formula derived in this work can guide the design and fine tuning of multilayered nanoparticles for the development of SERS and SEIRA in the MIR, as well as in-vivo imaging and theranostics using MIR wavelengths.

Funding

This research was funded by the Commonwealth of Australia, represented by the Australian Research Council through the Centre of Excellence for Transformative Meta-Optical Systems (CE200100010), as well as by the Defence Science and Technology Group, for the project-based funding agreement n.8673.

Disclosures

The authors declare that there are no conflicts of interest related to this article.

Data availability. Data underlying the results presented in this paper are not publicly available at this time but may be obtained from the authors upon reasonable request.

Supplemental document. See Supplement 1 for supporting content

References

1. N. G. Khlebtsov, L. Lin, B. N. Khlebtsov and J. Ye, "Gap-enhanced Raman tags: fabrication, optical properties, and theranostic applications," Theranostics, **10**(5), 2067 (2020).
2. H. L. Wang, E. M. You, R. Panneerselvam, S. Y. Ding and Z. Q. Tian, "Advances of surface-enhanced Raman and IR spectroscopies: from nano/microstructures to macro-optical design," Light: Science and Applications, **10**(1), 161, (2021).
3. A. Garcia-Etxarri and R. Yuste, "Time for NanoNeuro," Nature Methods, **18**(11), 1287-1293 (2021).
4. N. Hardy, A. Habib, T. Ivanov and A. A. Yanik. "NeuroSWARM3: Injectable electro-plasmonic nanosensors for wireless recording of the brain activity". in *Optics InfoBase Conference Papers*. (2021).
5. P. Singh, S. Roy, P. Sanpui, A. Banerjee and A. Jaiswal, "Gold nanostructures for photothermal therapy," in *Nanotechnology in Modern Animal Biotechnology: Recent Trends and Future Perspectives* (Springer, 2019).
6. M. Rosenberg and T. A. Petrie, "Theoretical study on the possible use of SiC microparticles as photothermal agents for the heating of bacteria," Nanotechnology, **23**(5), 055103, (2012).
7. M. Boksebeld, V. Kilin, A. Géloën, G. Ceccone, A. Jaffal, C. Schmidt, S. Alekseev, V. Lysenko, J. P. Wolf, L. Bonacina, E. Souteyrand, Y. Chevolot and V. Monnier, "Folate-modified silicon carbide nanoparticles as multiphoton imaging nanoprobes for cancer-cell-specific labeling," RSC Advances, **7**(44), 27361-27369 (2017).
8. R. Thangam, R. Paulmurugan and H. Kang, "Functionalized nanomaterials as tailored theranostic agents in brain imaging," Nanomaterials, **12**(1), 18, (2022).
9. B. Andreiuk, F. Nicolson, L. M. Clark, S. R. Panikkanvalappil, Kenry, M. Rashidian, S. Harmsen and M. F. Kircher, "Design and synthesis of gold nanostars-based SERS nanotags for bioimaging applications," Nanotheranostics, **6**(1), 10-30 (2022).
10. B. Guo, Y. Wang, C. Peng, H. L. Zhang, G. P. Luo, H. Q. Le, C. Gmachl, D. L. Sivco, M. L. Peabody and A. Y. Cho, "Laser-based mid-infrared reflectance imaging of biological tissues," Opt. Express, **12**(1), 208-219 (2004).
11. J. Song, Q. Cheng, Z. Luo, X. Zhou and Z. Zhang, "Modulation and splitting of three-body radiative heat flux via graphene/SiC core-shell nanoparticles," Int. J. Heat and Mass Transfer, **140**, 80-87 (2019).
12. D. Coleman and L. Mangolini, "Plasmonic core–shell silicon carbide–graphene nanoparticles," ACS Omega, **4**(6), 10089-10093 (2019).
13. B. Parida, J. Choi, G. Lim, K. Kim and K. Kim, "Enhanced visible light absorption by 3C-SiC nanoparticles embedded in Si solar cells by plasma-enhanced chemical vapor deposition," J. Nanomat., 953790, (2013).
14. W. Chen, C. Zou and X. Li, "An investigation into the thermophysical and optical properties of SiC/ionic liquid nanofluid for direct absorption solar collector," Solar Energy Materials and Solar Cells, **163**, 157-163 (2017).
15. W. Wu, M. Wan, P. Gu, Z. Chen and Z. Wang, "Strong coupling between few molecular excitons and Fano-like cavity plasmon in two-layered dielectric-metal core-shell resonators," Opt. Express, **25**(2), 1495-1504 (2017).
16. D. Paria, C. Zhang and I. Barman, "Towards rational design and optimization of near-field enhancement and spectral tunability of hybrid core-shell plasmonic nanoprobes," Scient. Rep., **9**(1), 1-9 (2019).
17. G. Ziegelberger, "ICNIRP statement on far infrared radiation exposure," Health Physics, **91**(6), 630-645 (2006).
18. D. Han, J. Xu, Z. Wang, N. Yang, X. Li, Y. Qian, G. Li, R. Dai and S. Xu, "Penetrating effect of high-intensity infrared laser pulses through body tissue," RSC Advances, **8**(56), 32344-32357 (2018).
19. M. Longmire, P. L. Choyke and H. Kobayashi, "Clearance properties of nano-sized particles and molecules as imaging agents: Considerations and caveats," Nanomedicine, **3**(5), 703-717 (2008).
20. J. Bourquin, A. Milosevic, D. Hauser, R. Lehner, F. Blank, A. Petri-Fink and B. Rothen-Rutishauser, "Biodistribution, Clearance, and Long-Term Fate of Clinically Relevant Nanomaterials," Adv. Mat., **30**(19), 1704307, (2018).
21. F. Huth, A. Govyadinov, S. Amarie, W. Nuansing, F. Keilmann and R. Hillenbrand, "Nano-FTIR absorption spectroscopy of molecular fingerprints at 20 nm spatial resolution," Nano Lett., **12**(8), 3973-3978 (2012).
22. D. C. Fernandez, R. Bhargava, S. M. Hewitt and I. W. Levin, "Infrared spectroscopic imaging for histopathologic recognition," Nat. Biotech., **23**(4), 469-474 (2005).
23. N. J. Bareza, K. K. Gopalan, R. Alani, B. Paulillo and V. Pruneri, "Mid-infrared gas sensing using graphene plasmons tuned by reversible chemical doping," ACS Photonics, **7**(4), 879-884 (2020).
24. J. D. Caldwell, L. Lindsay, V. Giannini, I. Vurgaftman, T. L. Reinecke, S. A. Maier and O. J. Glembocki, "Low-loss, infrared and terahertz nanophotonics using surface phonon polaritons," Nanophotonics, **4**(1), 44-68 (2015).
25. G. Dravecz, T. Z. Jánosi, D. Beke, D. Á. Major, G. Károlyházy, J. Erostyák, K. Kamarás and Á. Gali, "Identification of the binding site between bovine serum albumin and ultrasmall SiC fluorescent biomarkers," Phys. Chem. Chem. Phys., **20**(19), 13419-13429 (2018).
26. P. Rufangura, I. Khodasevych, A. Agrawal, M. Bosi, T. G. Folland, J. D. Caldwell and F. Iacopi, "Enhanced absorption with graphene-coated silicon carbide nanowires for mid-infrared nanophotonics," Nanomaterials, **11**(9), 2339, (2021).
27. N. Mishra, M. Bosi, F. Rossi, G. Salviati, J. Boeckl and F. Iacopi, "Growth of graphitic carbon layers around silicon carbide nanowires," J. Appl. Phys., **126**(6), 065304 (2019).
28. N. Mishra, J. Boeckl, N. Motta and F. Iacopi, "Graphene growth on silicon carbide: A review," Phys. Status Solidi A, **213**(9), 2277-2289 (2016).

29. F. Iacopi, N. Mishra, B. V. Cunning, D. Goding, S. Dimitrijev, R. Brock, R. H. Dauskardt, B. Wood and J. Boeckl, "A catalytic alloy approach for graphene on epitaxial SiC on silicon wafers," J. Mater. Res., **30**(5), 609-616 (2015).
30. T. Low and P. Avouris, "Graphene plasmonics for terahertz to mid-infrared applications," ACS Nano, **8**(2), 1086-1101 (2014).
31. A. Grigorenko, M. Polini and K. Novoselov, "Graphene plasmonics," Nat. Photonics, **6**(11), 749 (2012).
32. F. J. Garcia de Abajo, "Graphene plasmonics: challenges and opportunities," ACS Photonics, **1**(3), 135-152 (2014).
33. S. Bhardwaj, R. Uma and R. Sharma, "A study of metal@ graphene core–shell spherical nano-geometry to enhance the SPR tunability: influence of graphene monolayer shell thickness," Plasmonics, **12**(4), 961-969 (2017).
34. Y. Li, X. He, M. Wan, W. Wu and Z. Chen, "Unconventional Fano effect based spectrally selective absorption enhancement in graphene using plasmonic core-shell nanostructures," Appl. Phys. Lett., **109**(3), 031909 (2016).
35. D. T. Nurrohman and N. F. Chiu, "A review of graphene-based surface plasmon resonance and surface-enhanced raman scattering biosensors: Current status and future prospects," Nanomaterials, **11**(1), 216, 1-30 (2021).
36. D. Rodrigo, O. Limaj, D. Janner, D. Etezadi, F. J. G. De Abajo, V. Pruneri and H. Altug, "Mid-infrared plasmonic biosensing with graphene," Science, **349**(6244), 165-168 (2015).
37. T. Christensen, A.-P. Jauho, M. Wubs and N. A. Mortensen, "Localized plasmons in graphene-coated nanospheres," Phys. Rev. B, **91**(12), 125414 (2015).
38. S. Hayati Raad, Z. Atlasbaf, J. Rashed-Mohassel and M. Shahabadi, "Scattering from Graphene-Based Multilayered Spherical Structures," IEEE Trans. Nanotech., **18**, 8859634, 1129-1136 (2019).
39. C. Gao, B. Sun and Y. Zhang, "Electromagnetic wave scattering by charged coated spheres," Journal of Quantitative Spectroscopy and Radiative Transfer, **272**, 107757, (2021).
40. Comsol Multiphysics, "RF Module User's Guide."www.comsol.com
41. C. F. Bohren and D. R. Huffman, *Absorption and scatterign of light by small particles* (Wiley, 1983).
42. J. D. Jackson, *Classical Electrodynamics* (Wiley, 1999).
43. S. A. Maier, *Plasmonics: Fundamentals and applications* (Springer, 2007).
44. A. S. Barker Jr and M. Ilegems, "Infrared lattice vibrations and free-electron dispersion in GaN," Phys. Rev. B, **7**(2), 743-750 (1973).
45. J. D. Caldwell, A. V. Kretinin, Y. Chen, V. Giannini, M. M. Fogler, Y. Francescato, C. T. Ellis, J. G. Tischler, C. R. Woods, A. J. Giles, M. Hong, K. Watanabe, T. Taniguchi, S. A. Maier and K. S. Novoselov, "Sub-diffractional volume-confined polaritons in the natural hyperbolic material hexagonal boron nitride," Nat. Comm., **5**, 5221, (2014).
46. A. Pradeepkumar, M. Amjadipour, N. Mishra, C. Liu, M. S. Fuhrer, A. Bendavid, F. Isa, M. Zielinski, H. I. Sirikumara, T. Jayasekara, D. K. Gaskill and F. Iacopi, "p-Type Epitaxial Graphene on Cubic Silicon Carbide on Silicon for Integrated Silicon Technologies," ACS Applied Nano Materials, **3**(1), 830-841 (2019).
47. K. S. Novoselov, V. I. Fal'Ko, L. Colombo, P. R. Gellert, M. G. Schwab and K. Kim, "A roadmap for graphene," Nature, **490**(7419), 192-200 (2012).
48. V. Apalkov and M. I. Stockman, "Proposed graphene nanospaser," Light: Science and Applications, **3**, e191, (2014).
49. E. Prodan, C. Radloff, N. J. Halas and P. Nordlander, "A Hybridization Model for the Plasmon Response of Complex Nanostructures," Science, **302**(5644), 419-422 (2003).